Detecting magnetic field direction by a micro beam operating in different vibration modes*

Chen Jie(陈 洁), Qin Ming(秦 明), and Huang Qing-An(黄庆安)†

Key Laboratory of MEMS of Ministry of Education, Southeast University, Nanjing 210096, *China*

(Received 11 April 2011; revised manuscript received 11 May 2011)

A new method to detect the magnetic field direction by using a silicon structure is presented in this paper. The structure includes a micro beam and an in-plane coil electrode. When the electrode under a magnetic field is applied with an alternating current, the micro beam is actuated under the effect of the Lorentz forces. Magnetic fields of different directions cause different vibration profiles. The direction of the magnetic field is obtained by measuring the vibration amplitudes of the micro beam, which is driven to work at first- and second-order resonant modes. A micro structure has been fabricated using the bulk micromachined silicon process. A laser Doppler vibrometer system is implemented to measure the vibration amplitudes. The experimental results show that the amplitude of the structure, which depends on the different modes, is a sine or cosine function of the angle of the magnetic field. It agrees well with the simulation result. Currently a resolution of 10° for the magnetic field direction measurement can be obtained using the detecting principle.

Keywords: beam, micro-electro-mechanical systems, Lorentz force, resonance

PACS: 71.10.–w, 71.45.–d **DOI:** 10.1088/1674-1056/20/9/097101

1. Introduction

Magnetic sensors have assisted mankind in various fields, such as navigation, data storage, location sensing, foreign body detection, motion detection, current sensing, medical bio-electric detection and disease detection.[1,2] With the development of micro-electro-mechanical systems (MEMS), MEMS magnetic field sensors and MEMS magnetic field actuators[3] can not only reduce production costs, but also complete more projects than those of a larger size.

In the past few decades, the magnetic sensor market has been dominated by Hall effect devices and flux-gate magnetometers, which are cost-effective, batch-fabricated and can be easily integrated with electronics.[1] The known limitation of these sensors is their high power consumption. In recent years, many novel structures for magnetic field sensing have been introduced and analyzed by using micromachining technologies. To be small and cost-effective, these sensors are mostly fabricated by using the MEMS process, which is compatible with the complementary metal-oxide-semiconductor process and is known as CMOS-MEMS technology. New devices, such as resonant magnetic field microsensors, which use the Lorentz force to actuate the vibration of the suspended MEMS structures, are based on the measurement of electromechanical parameters, such as piezoresistance,[4−6] frequency[7] and vibration amplitude.[8] A resonant magnetic microsensor sensitive enough to measure the Earth's magnetic field for compass applications has been reported.[9−11] The sensor combined an electrostatically driven micromechanical resonator and a planar magnetic concentrator with two narrow gaps.

Information on the direction of the magnetic field is also required for the application of magnetic field measurement. A device composed of a permanent magnet integrated with a rotational comb drive resonator can be used to measure the direction of an external magnetic field.[12−14] The shift of the fundamental mechanical resonant frequency of the device caused by the interaction of the external magnetic field with the magnetic component of the resonant system is used to determine the amplitude or the direction of the external field. The realization of very small resonators is usually a challenge, because it is difficult to fabricate a miniaturized permanent magnet.

In this paper, an approach to build a Lorentz-force-driven structure using micromachining technology is proposed. The sensor consists of a resonating structure incorporated into an aluminum planar conductive coil. The interaction of the electrically con-

*Project supported by the National Natural Science Foundation of China (Grant No. 61076071).

†Corresponding author. E-mail: hqa@seu.edu.cn

© 2011 Chinese Physical Society and IOP Publishing Ltd

ductive lines with an external magnetic field alters the vibrational modes of the structure,[15,16] thereby allowing a readout of the direction of the external field.

The bulk micromachined process was used to fabricate the sensing structure. Both theoretical analysis and finite element analysis (FEA) were performed to find the best configurations of the electric excitation. Experimental validation was conducted using a laser Doppler vibrometer system. The measurement of the magnetic field direction as well as the amplitude has been demonstrated.

2. Operating principle

As shown in Fig. 1, the mechanical structure of the magnetic sensor consists of a freestanding membrane supported by two micro beams. An aluminum planar coil used for magnetic coupling runs along the periphery of the membrane. The driving current with a magnetic field presented results in different Lorentz forces on different sides of the membrane. The interaction of the aluminum planar coil with an external magnetic field alters the vibrational amplitude of the membrane, thereby allowing the readout of the direction of the external field. A variation of the frequency of the drive current will result in the change of the vibration amplitude of the membrane. The membrane vibration can be considered as a time-variant weighted superposition of its resonant mode functions. If the frequency of the current approaches one of the resonant frequencies, the membrane will resonant greatly at that resonant mode, making the vibration amplitude large enough to be observed.

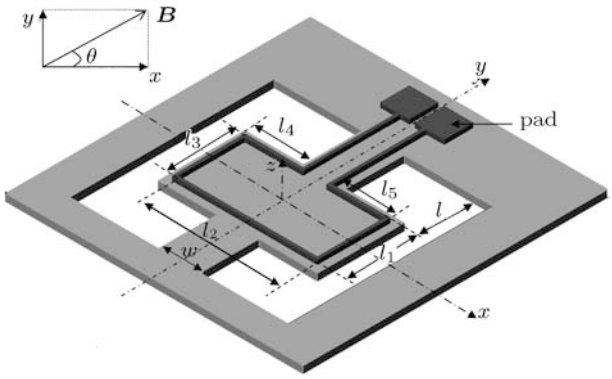


Fig. 1. Schematic of magnetic field detection.

Neglecting the minor geometric asymmetry of the sensing structure, there are two major sets of resonant modes of vibration in the structure. One set are the y-axis anti-symmetric resonant modes, in which the membrane rotates about the y axis. The other set are the x-axis symmetric resonant modes, in which the membrane symmetrically rotates out-of-plane about the x axis. It is clear that the former set is contributed by the Lorentz forces from the x component of the magnetic field and the latter set by those from the y component. In each set, the first-order resonant mode of vibration is most significant, because the response of higher orders shrinks dramatically with the increased frequency. We denote the first-order modes of the y-axis anti-symmetric modes and the x-axis symmetric modes as YAS1 mode and XS1 mode, respectively. The responses of these two modes at resonance are used to detect the amplitude and the direction of the magnetic field.

Assume the clockwise current to be positive. When the frequency of the forcing current is sinusoidally driven to the first resonant frequency of the mechanical structure, the displacement at the edge of the membrane for the YAS1 mode can be written as

$$A_1(t) = \frac{F_1(t)}{k_1} Q_1 = \frac{-F_3(t)}{k_1} Q_1, \tag{1}$$

where Q_1 is the quality factor of the resonant rotation, k_1 is the stiffness coefficient of the y-axis torsion, and $F_1(t)$ and $F_3(t)$ are the Lorentz forces acting on metal lines l_1 and l_3, respectively. For driving current I and external field B, they are given by

$$F_1(t) = -F_3(t) = I l_1 B \cos\theta \sin 2\pi f_1 t, \tag{2}$$

where l_1 is the length of the line, f_1 is the resonant frequency of the YAS1 mode, θ is the angle between the direction of the external field and the x axis. The amplitude of rotation about the y axis can thus be obtained as

$$A_{1\mathrm{p}} = \frac{2 I l_1 B \cos\theta}{k_1} Q_1. \tag{3}$$

The stiffness coefficient of torsion can be expressed as[17]

$$k_1 = \frac{2 G I_{\mathrm{p}}}{l}, \tag{4}$$

where G is the shear modulus, I_{p} is the polar moment of inertia and l denotes the length of the torsional micro beam.

The following equation can be used for the quality factor of the resonant rotation,[18]

$$Q_1 = \frac{(2\pi)^{1/2}}{8\pi} \frac{\omega_1 \rho d}{P} \left(\frac{R_0 T}{M}\right)^{1/2}, \tag{5}$$

where ω_1 is the circular resonant frequency of the YAS1 mode, M is the molar mass of air, R_0 is the universal gas constant, T is the absolute temperature, P is the pressure, d is the thickness of the resonator and ρ is the density of the structural material.

Following a similar procedure as above, an approximation to the maximum amplitude of the XS1 mode $A_{2\mathrm{p}}$ can be given as

$$A_{2\mathrm{p}} = \frac{I\,(l_2 - l_4 - l_5)\,Q_2}{k_2} B \sin\theta, \tag{6}$$

where Q_2 is the quality factor of bending, k_2 is the stiffness coefficient of bending, l_2, l_4 and l_5 are the lengths of the metal lines as shown in Fig. 1. The stiffness coefficient of bending k_2 can be expressed as[17]

$$k_2 = \frac{24EI_{\mathrm{i}}}{l^3}, \tag{7}$$

where E is the Young's modulus and I_{i} is the cross-sectional inertia of the torsion beam. The quality factor of bending can be expressed as[19]

$$Q_2 = (2\pi)^{\frac{3}{2}}\,\rho d\omega_2 \left(\frac{h_0}{s}\right)\sqrt{\frac{RT}{M}}\,\frac{1}{P}, \tag{8}$$

where ω_2 is the circular resonant frequency of the XS1 mode, h_0 is the nominal gap between the membrane and the substrate, and s is the peripheral length of the gap.

A 90° phase shift between the modes of the YAS1 and the XS1 is detected at the mechanical resonance modes. The maximum amplitudes of the beam are determined by the angle, which is defined so that it is zero when $\boldsymbol{B}$ is parallel to the x axis (see Fig. 1). When the magnetic field is applied in the direction parallel to the x axis, the YAS1 amplitude $A_{1\mathrm{p}}$ is obtained. When it is applied parallel to the y axis, the XS1 amplitude $A_{2\mathrm{p}}$ is obtained. Angle θ of a magnetic field in an arbitrary direction can thus be calculated using

$$\theta = \mathrm{arctg}\left(k\frac{A_{2\mathrm{p}}}{A_{1\mathrm{p}}}\right), \tag{9}$$

where k is the normalized coefficient that compensates for the difference of the mode responses under the same magnetic field. According to Eqs. (3) and (6), it can be written as

$$k = \frac{k_2 Q_1}{k_1 Q_2} \cdot \frac{2l_1}{l_2 - l_4 - l_5}. \tag{10}$$

3. Simulation

To validate the operation principle, the resonant frequencies and the modes of the resonators were simulated using the finite element program ANSYS. The mechanical properties including Young modulus E, Poisson's Ratio ν, density ρ and thickness h of different thin-film materials are summarized in Table 1. Table 2 lists the geometrical dimensions of the sensing structure. The dimensions were measured using an HIROX KH-3000VD 3-D microscope. In the simulation, the constant damping ratios were set to 0.005 for the YAS1 mode and 0.0017 for the XS1 mode.

The simulated mode shapes of the two lowest modes for the resonator are shown in Fig. 2. As expected, the YAS1 mode corresponds to a rotation

Table 1. Material properties used for FEM simulation.

Material	$E/10^9$ Pa	ν	ρ/g·cm^{-3}	h/μm
Polysilicon	160	0.22	2300	10
Silicon oxide	73	0.17	2500	0.3
Aluminum	70	0.33	2700	0.8

Table 2. Geometries used for FEM simulation.

Length/μm		Width/μm		
l_1	l	l_2	l_4	w
600	400	1100	400	340

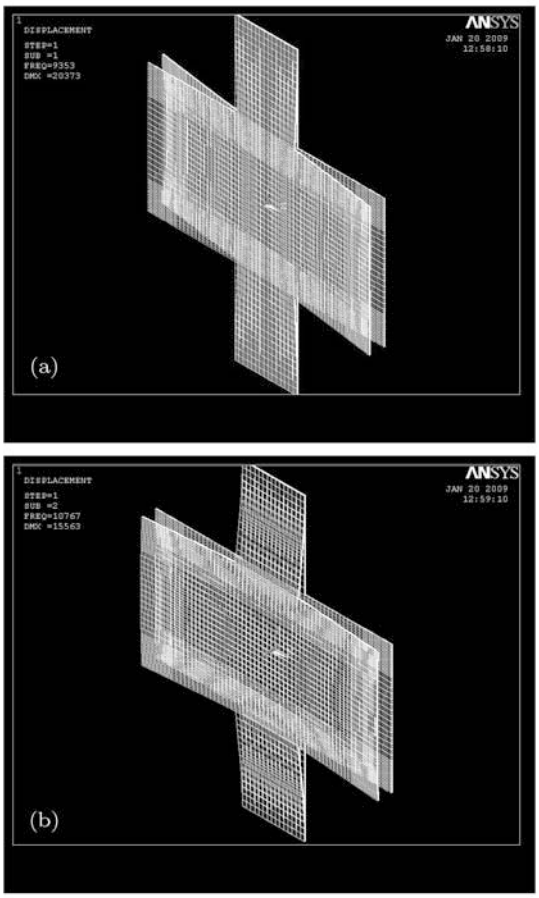


Fig. 2. Resonant mode shapes of the structure: (a) the 1st mode, shape of the rotation about an axis; (b) the 2nd mode, shape of the out-of-plane vibration.

about the y axis and the XS1 mode vibrates out-of-plane, which is a mode with a nodal line perpendicular to the clamped side. The difference between their phases is exactly 90°.

Figure 3 shows the plot of the simulated maximum amplitudes of the structure under magnetic fields of 60 mT and 80 mT as a function of the field direction. The results agree well with the theoretical prediction. The maximum amplitude linearly increases with the increasing magnitude of the magnetic field. The YAS1 response reaches its maximum/minimum when the XS1 response reaches its minimum/maximum, leading to a phase difference of 90° in the amplitude–direction diagram, as shown in Fig. 3. In addition, a clear sine curve is observed with the simulated maximum amplitude proportional to $\boldsymbol{B}$. The simulated maximum amplitude of the first mode is about five times larger than that of the second mode.

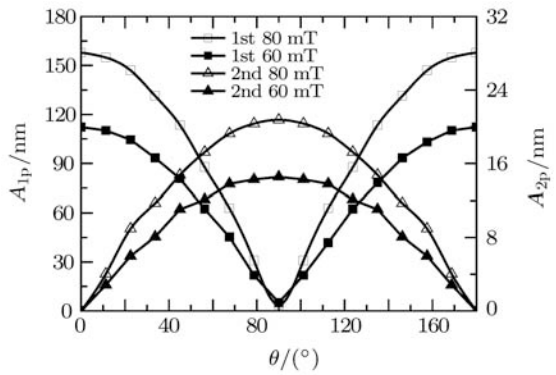


Fig. 3. Simulated maximum amplitudes of the two modes of the sensor.

4. Fabrication

As shown in Fig. 4, the starting material was a 4″ (100) p-type silicon wafer. Firstly, an approximately 8 μm-thick N-doped layer (Fig. 4(a)) was formed by phosphorus diffusion. The layer was used as the structural layer and was released by the pn junction etch-stop and dry-etch methods. After diffusion, 1 μm-thick thermal SiO_2 was thermally grown on the surface as the insulator (Fig. 4(b)). Next, an approximately 500 nm-thick aluminum film was sputtered on the surface and patterned to form the coil and the wire bonding pad (Fig. 4(c)). Then, electrochemical wet etching on the backside of the wafer was performed to obtain the n-type silicon layer (as shown in Fig. 4(e)). Finally, the structure was released by inductively coupled plasma etching of the n-type silicon layer (as shown in Fig. 4(f)). A typical test structure is shown in Fig. 5.

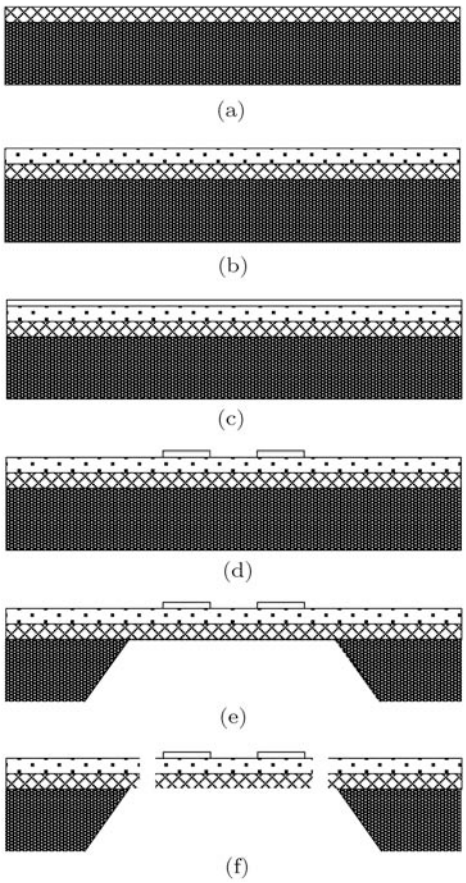


Fig. 4. Fabrication process of the structure: (a) diffusion, (b) oxidation, (c) metal plating, (d) wire etching, (e) wet etching and (f) ICP etching.

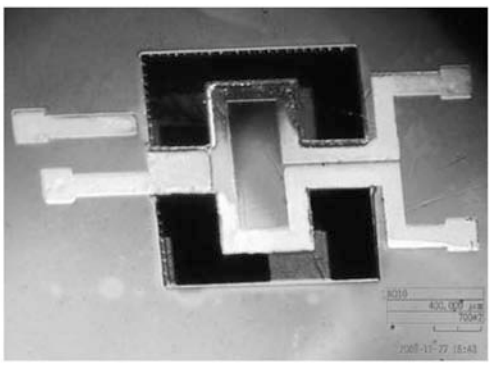


Fig. 5. Photo of a typical test structure.

5. Measurements and results

The vibration amplitudes of the micromachined structures were detected by using a laser Doppler vibrometer (LDV). The LDV is capable of measuring the frequency spectrum of the vibrating object under the laser spot via the Doppler effect.[20] A Polytech LDV system with hardware modules of MSV-400-M2

was used in this experiment.[21] The setup of the LDV system is shown in Fig. 6. In the measurement, an alternating current (AC) voltage up to 300 mV in amplitude was applied across the coil under a magnetic field. Frequency spectra at the edge of the vibrating membrane were measured, from which the resonant frequencies were extracted.

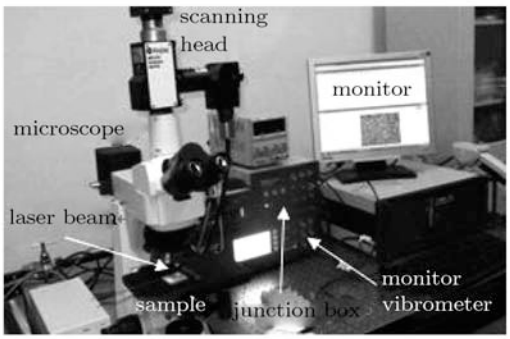


Fig. 6. Configuration of the LDV system. The system mainly consists of a scanning head to control the laser scanning, a vibrometer to decode the laser signal and a junction box to interconnect each part.

Figure 7 shows the response spectrum. The first two peaks correspond to the YAS1 and the XS1 modes, respectively. The FEM results are compared with the experimental data. The simulated and the experimentally detected resonant frequencies of the structure are summarized in Table 3. Experimental data are in agreement with the calculated values within an error of 7%. Other important parameters of the two mode vibrations were also measured experimentally, including stiffnesses $k_1 \approx 130$, $k_2 \approx 370$ and quality factors $Q_1 \approx 100$, $Q_2 \approx 310$. The applied magnetic field generated by a permanent magnet was independently measured by using an external Gauss meter. All measurements were performed at atmospheric pressure.

Table 3. Four lowest experimentally detected and simulated resonance frequencies of the structure.

	$f_{\rm exp}$/kHz	$f_{\rm ansys}$/kHz	$f_{\rm ansys}/f_{\rm exp}$
f_1	23.1	22.9	1.008
f_2	25.3	26.9	0.941
f_3	78.4	80.5	0.974
f_4	86.1	83.7	1.028

Figure 8 shows the dependence of the vibration amplitudes on the angle under an external magnetic field of 80 mT. As expected, the vibration amplitudes of the YAS1 and the XS1 modes show a sinusoidal dependency on the applied magnetic field angle. The simulated results fit well with those of the measured data and validate the operation principle of the sensing structure. Figure 9 plots the measured angles as a function of the applied angle. It can be estimated that a minimum resolution of 10° has been achieved at the current stage of design. This sensing technique maintains the measurement precision of the magnetic field direction while reducing the sensing structure to the minimum size.

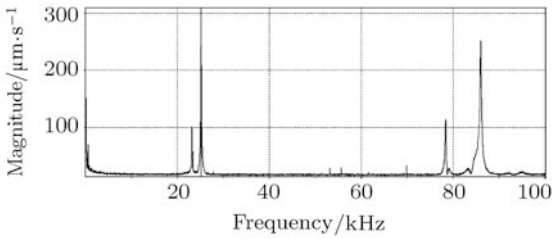


Fig. 7. Experimentally detected resonance frequencies of the structure.

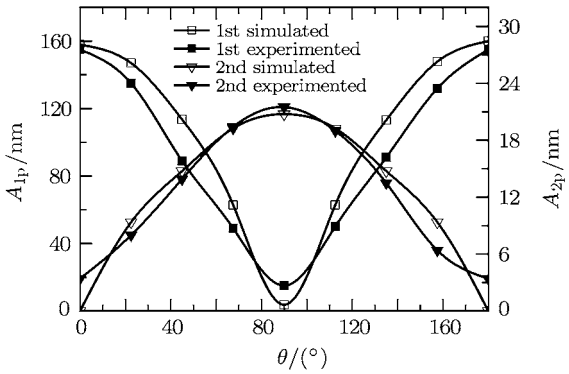


Fig. 8. Experimental and simulated amplitudes of the structure as a function of the direction of the applied magnetic field. Magnetic field intensity is 80 mT.

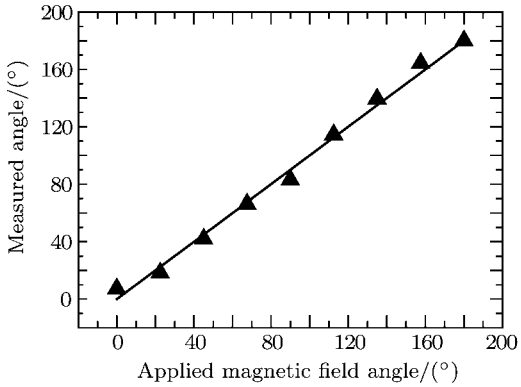


Fig. 9. Measured angle as a function of the direction of the magnetic field.

6. Conclusion and discussion

A miniaturized sensing structure has been designed and fabricated to measure the direction of magnetic field. The altering Lorentz forces on each side of the coil drive the membrane to vibrate in resonance.

The direction of the magnetic field is obtained according to the amplitudes of the two resonant vibrations, respectively, driven by the orthogonal components of the magnetic field. The proof-of-concept structure was simulated using finite element analysis and was fabricated using the bulk-micromachined process. The designed test structure has achieved a resolution of 10° for field direction measurement at 80 mT. The experimental data is consistent with the theoretical analysis and thus validates the concept of the design.

The Lorentz force applied to the coils of the support beam can deform the structure. However, it is found in the calculation that the deformation is small relative to that caused by the coils around the perimeter of the board, thus it is negligible. This conclusion is consistent with the results given by the simulation.

Acknowledgement

The authors wish to acknowledge the assistance and support of the MEMS Laboratory of the Southeast University.

References

[1] Lenz J E 1990 *Proc. IEEE* **78** 973

[2] Yang G, Tu B H, Li G H, Zhao H W and Zhou S P 2008 *Chin. Phys.* B **17** 1674

[3] Fang Y M, Huang Q A and Li W H 2008 *Chin. Phys.* B **17** 1715

[4] Baglio S, Latorre L and Nouet P 1999 *Proceedings of the 16th IEEE of Instrumentation and Measurement Technology Conference*, May 24–26, 1999 Venice, Italy, p. 452

[5] Beroulle V, Bertrand Y, Latorre L and Noue P 2003 *Sens. Actuators* A **103** 23

[6] Dumas N, Azais F, Latorre L and Nouet P 2005 *Proceedings of the 23rd IEEE VLSI Test Symposium*, May 1–5, 2005 Palm Springs, USA, p. 213

[7] Sunier R, Vancura T, Li Y, Kirstein K and Baltes H 2006 *J. Microelectromech. Syst.* **15** 1098

[8] Eyre B, Pister K S J and Kaiser W 1998 *IEEE Electron Device Lett.* **19** 496

[9] Brugger S, Simon P and Paul O 2006 *Proceedings of the 5th IEEE Conference on Sensors*, October 22–25, 2006 Daegu, Korea, p. 1016

[10] Brugger S and Paul O 2008 *Proceedings of the IEEE 21st Annual International Conference on Micro Electro Mechanical Systems,* January 13–17, 2008 Tucson, USA, p. 944

[11] Brugger S and Paul O 2009 *J. Microelectromech. Syst.* **18** 1432

[12] Leichle T C ,Ye W and Allen M G 2003 *Proceedings of the IEEE 16th Annual International Conference on Micro Electro Mechanical Systems,* January 19–23 , 2003 Kyoto, Japan, p. 514

[13] Leichle T C, Arx M V, Reiman S, Zana I, Ye W and Allen M G 2004 *J. Micromech. Microeng.* **14** 462

[14] Choi S, Kim S H, Yoon Y K and Allen M G 2006 *IEEE Trans. Mag. Conf.* **42** 3506

[15] Chen J, Huang Q A and Qin M 2009 *Proceedings of the 8th IEEE Conference on Sensors,* October 25–28, 2009 Christchurch, New Zealand, p. 1246

[16] Chen J, Qin M and Huang Q A 2011 *Proceedings of the 16th International Conference on Solid-State Sensors, Actuators and Microsystems,* June 5–9, 2011 Beijing, China, p. 1108

[17] Zhao J P, Chen H L, Huang J M and Liu A Q 2005 *Sens. Actuators* A **120** 199

[18] Kadar Z, Kindt W, Bossche A and Mollinger J 1996 *Sens. Actuators* A **53** 299

[19] Bao M H and Yang H 2007 *Sens. Actuators* A **136** 3

[20] Ozdoganlar O B, Hansche B D and Carne T G 2005 *Exp. Mech.* **45** 498

[21] Song J, Huang Q A, Li M and Tang J Y 2009 *J. Microelectromech. Syst.* **18** 274